



Accelerated crystallization of poly(L-lactic acid) by silk fibroin nanodisc

Amit Kumar Pandey¹ · Vimal Katiyar² · Sono Sasaki¹ · Shinichi Sakurai¹

Received: 4 May 2019 / Revised: 12 June 2019 / Accepted: 12 June 2019 / Published online: 9 July 2019
© The Society of Polymer Science, Japan 2019

Abstract

Slow crystallization of poly(L-lactic acid) (PLLA) limits the widespread applications of PLLA because of its insufficient thermal and mechanical properties. In this study, a biobased filler, silk fibroin nanodisc (SFN), has been included in the PLLA matrix with the aim of accelerating the crystallization process of PLLA. Detailed investigation of the effect of SFN inclusion on the crystallizability of PLLA has been performed by polarizing optical microscope (POM) observations and differential scanning calorimetry (DSC) measurements. For isothermal crystallization studies by DSC, extremely quick cooling (~300 °C/min) from the melt to the crystallization temperature was conducted in order to avoid nucleation during the cooling process. The experimental results show that the small amount of SFN (only 1%) can significantly enhance the crystallizability of PLLA. The glass transition temperature and the melting temperature of PLLA were not influenced by the inclusion of SFN. However, the nucleation rate and the final degree of crystallinity were significantly enhanced. The effect of optical purity on the acceleration ability of SFN was examined in this research by utilizing two different types of PLLA having different contents of the D moiety (0.5 and 1.4%). As a result, it was found that the extent of enhancement is much larger in the case of highly optical pure PLLA (0.5% D moiety).

Introduction

Poly(L-lactic acid) (PLLA) is one of the most popular biobased polymers. It is synthesized from the monomer L-lactic acid, which is obtained from 100% natural resources. Over the past decades, PLLA has become an impressive material as a potential replacement for petroleum-based polymers. PLLA is advantageous due to its high mechanical strength; however, its industrial applications are limited because of its inferior properties such as slow nucleation and crystallization rate, low degree of crystallinity, and low thermal stability. The study of PLLA crystallization is of great importance as improved crystallization may be able to enhance its thermal and mechanical properties, including the gas-barrier properties as a notable example [1].

To accelerate the crystallization of PLLA, several strategies have been employed by researchers [2–9]. The addition of a nucleating agent is one of the simplest, yet most effective, methods. Most of the nucleating agents reported for PLLA (talc, carbon nanotubes, graphene, and clay [2–6]) are inorganic materials that are nonbiodegradable in nature.

The nucleation ability of a filler is highly related to the chemical and crystallographic matching between the filler and the matrix polymer. Therefore, it is meaningful to look for fillers with a chemical structure similar to PLLA. In this regard, poly(L-alanine) is a good candidate because of the similarity in chemical structure, as shown in Fig. 1. The size of the filler also plays a key role in the enhancement of the nucleation of polymers. Conventional fillers, such as talc, are usually in the micrometer range. Nanoscale fillers have gained significant interest recently, as only a small amount of the filler is required to be included in the polymer matrix [5–7].

Natural silk consists of a β -sheet crystalline domain, which contains a significant amount of poly(L-alanine), depending on the animal species that produces the silk [10]. In case of the muga silk, the L-alanine content is ~33.3% [11] and the other amino acids present are serine (13.2%) and glycine (30%). After completing acid hydrolysis, the

✉ Shinichi Sakurai
shin@kit.ac.jp

¹ Department of Biobased Materials Science, Kyoto Institute of Technology, Kyoto 606-8585, Japan

² Department of Chemical Engineering, Indian Institute of Technology Guwahati, Guwahati 781039 Assam, India

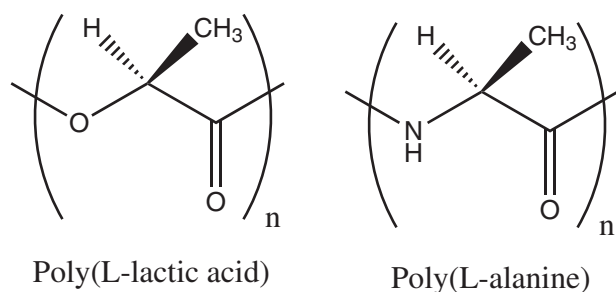


Fig. 1 Chemical structures of poly(L-lactic acid) and poly(L-alanine). L-Alanine is the main component (83.8%) of the silk fibroin nanodisc

amorphous part of the silk fibroin was removed and only the amino acids that were present in the crystalline domain (β -sheet) remained. Thus, the obtained extract is composed of 83.8% L-alanine, 6.8% serine, and 6.1% glycine [11].

Very recently, Patwa et al. [12, 13] reported that the silk fibroin nanodisc (SFN) has the potential to increase the crystallizability of PLLA. They attempted to study the effect of SFN on the crystallization behavior of PLLA. In their study, specimens were prepared by using melt extrusion at high temperature (210 °C), which unfortunately resulted in the degradation of PLLA due to such high temperature and mechanical shearing during the processing. This is a very severe drawback for the study of the crystallization of PLLA that has been identified by other researchers as well [14]. Due to thermal degradation, the molecular weight is decreased, which affects the crystallization behavior. Although they concluded that the crystallization behavior was improved by SFN, their results may have suffered from the effects of the degradation due to the specimen preparation method (the melt extrusion). Thus, the effect of SFN is still unclear. To clearly examine the effect of SFN, we prepared specimens by the solution casting method. Although the solution casting method is not industrially feasible, this technique is much more favorable than melt extrusion for the fundamental study of crystallization.

Experimental section

Specimens

The PLLA used in this study was obtained from Nature-Works LLC, USA. The sample characteristics are summarized in Table 1. SFN is a nanoparticle that was prepared in the laboratory from the waste of the muga silk (*Antheraea assama*) cocoon by the acid hydrolysis method [11–13]. The crystalline portion (the β sheets of the silk fibroin) was isolated, and well-defined disc-like particles were obtained. Such morphology and dimensions have been reported previously [11–13], as 20–80 nm in diameter (with an average

Table 1 Sample characterization

| Sample code | Abbreviation | D content | Number-average molecular weight (M_n) |
|-------------|--------------|-----------|---|
| PLLA 4032D | D1.4 | 1.4% | 1.66×10^5 |
| PLLA 2500HP | D0.5 | 0.5% | 1.74×10^5 |

diameter of ~45 nm) and 2–5 nm in thickness. The degree of crystallinity in SFN was calculated from X-ray diffraction data as ~93.7%. The SFN is thus hydrophobic and biocompatible [11–13].

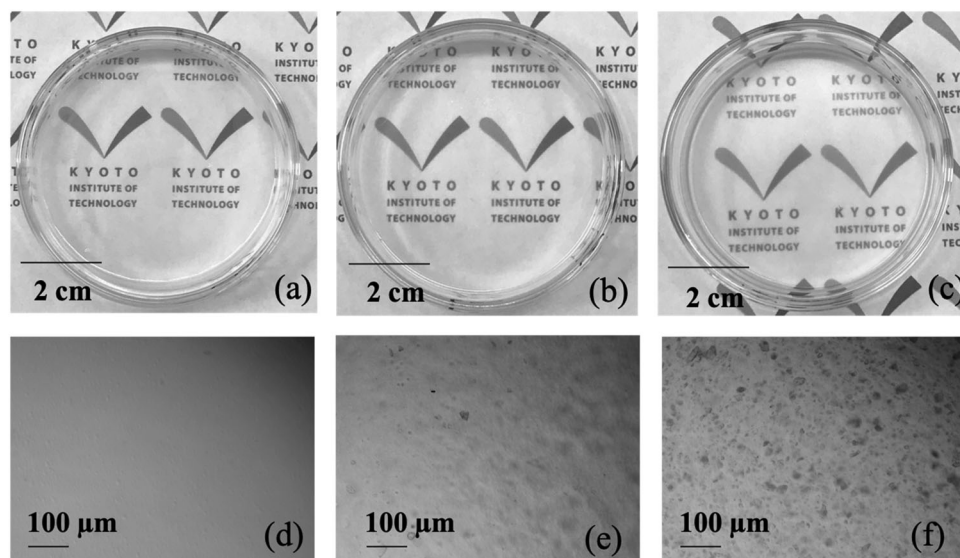
Preparation of PLLA/SFN specimens

Prior to the solution casting, PLLA pellets and SFN powder were dried in a vacuum oven at 50 °C for 24 h. The dried SFN was dispersed in dichloromethane (DCM). After 1 h of mixing by magnetic stirring, the SFN dispersion was sonicated at RT for 30 min and 40 kHz by using an ultrasonic water bath sonicator (VS-25, Velvo-Clear Ltd, Osaka, Japan). Since the water bath temperature increased during the sonication process, which may cause evaporation of DCM (boiling point = 39.6 °C), the water in the ultrasonic bath was refreshed every 5 min to maintain the bath temperature. Next, PLLA was added to the SFN dispersion to make the PLLA concentration 5% (w/v). After complete dissolution of PLLA, the solution was poured in a glass Petri dish for solvent evaporation at RT. After complete evaporation of the solvent, the films were further dried in a vacuum oven at 50 °C for 24 h. Films with a thickness of ~100 μ m were obtained. The specimens were labeled as D1.4/SFN(x) or D0.5/SFN(x), where the numbers after the D denote the % of D moiety in PLLA, and x stands for the percent of SFN inclusion. The color and transparency of the films are shown in Fig. 2. The film with 2-wt% inclusion of SFN shows the aggregation of SFN (Fig. 2c, f) with a typical aggregation size of 5–35 μ m in diameter. Since the SFN aggregates in the as-cast PLLA film for the case of 2-wt% inclusion, the current study mainly focuses on the case of 1-wt% SFN inclusion. It should be noted, however, that a few aggregates with 10–20- μ m diameters are discernible in Fig. 2e even for the case of the 1-wt% SFN inclusion, although they are far fewer in quantity.

Differential scanning calorimetry (DSC) measurement

DSC measurements for nonisothermal crystallization were performed by using a Shimadzu DSC-60 Plus instrument (Shimadzu, Kyoto, Japan), under nitrogen purge (50 ml min⁻¹). First, the specimens were melted at 200 °C for 5 min to erase thermal history and then cooled to RT at the rate of 10 °C/min

Fig. 2 Color and transparency of specimens **a** D1.4 neat **b** D1.4/SFN(1.0) **c** D1.4/SFN(2.0). **d–f** Showing magnified images of the same specimens for **(a)–(c)**



or 5 °C/min. The second heating run was conducted from RT to 200 °C at the rate of 10 °C/min.

As for the isothermal crystallization study by DSC, the cooling of the specimen from the melt to a given crystallization temperature is required to be performed as quickly as possible. For this purpose, the conventional DSC apparatus is useless because of the moderate cooling rate available. We used a special type of DSC apparatus (DSC214 *Polyma*, NETZSCH, Germany) equipped with a liquid nitrogen cooling system. The DSC was calibrated with an Indium standard for the temperature and heat flow. First, specimens were melted at 200 °C under nitrogen purge for 5 min and quickly cooled (the cooling rate was 300 °C/min) to a given isothermal crystallization temperature (90, 100, 105, 110, 120, 125, and 130 °C) and the DSC measurement was continued until the crystallization was complete. After the isothermal crystallization, the specimens were heated to 200 °C with a heating rate of 10 °C/min to measure the melting temperature of the PLLA crystallites formed in the isothermally crystallized specimens. Note that a fresh specimen was used for each measurement in order to eliminate unfavorable thermal degradation.

POM observation

POM observations were conducted by using a Nikon Eclipse *Ci-POL* POM equipped with the Linkam THMS600 hot stage (Linkam Scientific, UK) to observe spherulites and to evaluate the growth rate of spherulites. The specimens were sandwiched between two cover slips. Next, the specimens were melted on a hot stage at 200 °C for 3 min, then quickly cooled (cooling rate = 150 °C/min) to the isothermal crystallization temperature (T_{iso}) of 120 °C, and

then kept isothermally until the completion of the crystallization process. The POM images were taken under crossed polarizers with a 530 nm optical retardation plate inserted in the optical path.

Results and discussion

Nonisothermal crystallization by DSC

Figure 3 shows the DSC cooling and reheating thermograms of the D1.4 neat, D1.4/SFN(1.0), D0.5 neat and D0.5/SFN(1.0) specimens. The DSC results are summarized in Table 2. As shown in Fig. 3a, upon cooling from 200 °C to RT at a rate of 10 °C/min, no crystallization exothermic peak was observed for the case of the D1.4 specimens. However, the D0.5 specimens show an exothermic peak around 102 °C during the cooling scan (10 °C/min). This is due to the difference in the optical purity of the specimens. It is well known that the presence of the D moiety decreases the crystallizability of PLLA [1]. In the subsequent heating, the glass transition temperature (T_g) was observed clearly around 60 °C (Table 2). The T_g values for the D1.4 specimens and D0.5 specimens are almost the same. This indicates that the T_g of PLLA does not significantly depend on the D moiety [1]. The result that T_g does not change with the inclusion of SFN is also noteworthy.

Since the cooling rate of 10 °C/min is too fast for the D1.4 specimens to crystallize, we conducted nonisothermal crystallization with a slower cooling rate (5 °C/min) to induce crystallization during the cooling scan from the melt. The results are shown in Fig. 3c. For this condition, the exothermic peak appears at 97.8 °C for the D1.4 neat specimen and 98.0 °C for the D1.4/SFN(1.0) specimen.

Fig. 3 DSC curves of **a** cooling scans with a rate of 10 °C/min **b** the subsequent heating scans with a rate of 10 °C/min, and **c** the independent cooling scans with a rate of 5 °C/min

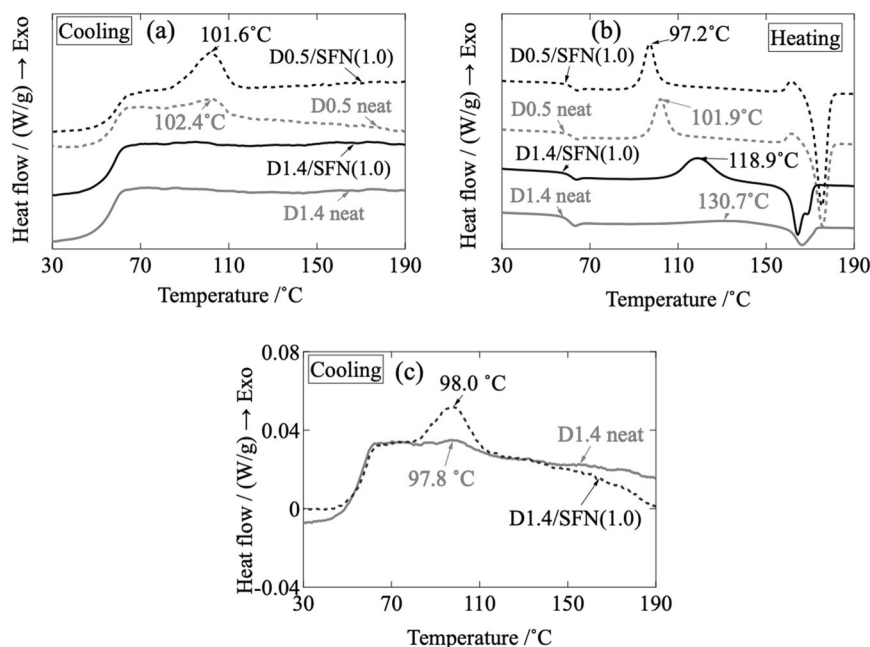


Table 2 DSC results for the nonisothermal crystallization

| Specimens | Heating scan | | | | | Cooling scan (10 °C/min) | | Cooling scan (5 °C/min) | |
|----------------|--------------|---------------|-----------------------|--------------|--------------------|--------------------------|--------------------|-------------------------|--------------------|
| | T_g (°C) | T_{cc} (°C) | ΔH_{cc} (J/g) | T_m (°C) | ΔH_m (J/g) | T_c (°C) | ΔH_c (J/g) | T_c (°C) | ΔH_c (J/g) |
| D1.4 neat | 59.6 | 130.7 | 16.6 | 166.5 | 16.8 | – | – | 97.3 | 1.1 |
| D1.4/SFN (1.0) | 60.1 | 118.9 | 35.1 | 164.5, 168.5 | 38.2 | – | – | 98.0 | 4.6 |
| D0.5 neat | 60.6 | 101.9 | 36.5 | 175.5 | 44.3 | 102.4 | 2.4 | – | – |
| D0.5/SFN (1.0) | 60.7 | 97.2 | 37.2 | 175.2 | 48.5 | 101.6 | 5.9 | – | – |

Although there is no clear effect of SFN on the value of T_c , a 4.5-fold larger ΔH_c was attained by loading SFN. For the results of the subsequent heating after the cooling at a rate of 10 °C/min (Fig. 3b), the lower T_{cc} (cold crystallization temperature) for the 1% SFN loading sample indicated improved crystallizability. Furthermore, the larger ΔH_{cc} values are noteworthy.

It is notable to observe that for the case of the D0.5 neat and D0.5/SFN(1.0) specimens an exothermic peak (peak area = 4.3 J/g) was observed (Fig. 3b) at 161.4 °C just before the endothermic melting peak. No such peak was observed for the case of the D1.4 neat and D1.4/SFN(1.0) specimens. These results indicate the transition of the α' -to- α phase during the heating scans [15–17]. For the D1.4/SFN(1.0) specimen, double melting peaks were observed. The low and high temperature melting peaks (164.5 and 168.5 °C) correspond to the melting of α' and α crystals, respectively. Such distinct melting behavior of the specimens can be explained by taking a look at T_{cc} in the heating scans. According to

references [15, 18, 19], mainly α crystals of PLLA are formed when the T_{iso} is higher than 120 °C. At 100 °C < T_{iso} < 120 °C, both α and α' crystals are formed. In case of T_{iso} < 100 °C, mainly α' crystals are formed. As shown in Fig. 3b, for the D0.5 neat and D0.5/SFN(1.0) specimens, the T_{cc} values are 101.9 °C and 97.2 °C, respectively. Therefore, α' crystals are formed for these specimens. Upon heating, the α' crystals are subjected to transformation into α crystals. As a matter of fact, such transformation was seen at 161.4 °C by observing the exothermic peak for both the D0.5 neat and the D0.5/SFN(1.0) specimens. In contrast, the T_{cc} of the D1.4 neat specimen (130.7 °C) is higher than 120 °C so that α crystals are formed. The fact that there is no exothermic peak due to the α' -to- α transition for the D1.4 neat specimen confirms the direct formation of the α crystals during the heating scan. For the D1.4/SFN(1.0) specimen, the T_{cc} value is 118.9 °C, and therefore, a mixture of α' and α crystals is formed. This may be the reason why double melting peaks are observed around 165 °C with endothermic peaks appearing in

a lower and a higher temperature being assigned to α' and α crystals, respectively.

POM observation

POM observations were conducted to evaluate the spherulite growth rate and the nucleation density as a function of time. The representative images of the evolution of spherulites for the D1.4 neat and D1.4/SFN(1.0) specimens at 120 °C as a function of time are shown in Fig. 4. First, negative spherulites were observed for both of the D1.4 neat and D1.4/SFN(1.0) specimens, indicating that SFN has no effect on the formation of negative spherulites without the extinction ring. As shown in Figs. 4a and 5b, the number of spherulites increases as a function of time for the D1.4 neat specimen below 14 min, suggesting homogeneous nucleation. In contrast, for the case of D1.4/SFN(1.0), the number of spherulites first rapidly increases and then becomes constant after 3.9 min (Fig. 5b), suggesting heterogeneous nucleation due to the nucleation effect of SFN. The slope of the plots in Fig. 5b can be considered as the rate of nucleation (N). Judging from the slope, it was found that in the early stage, N increases from 0.36 to 3.9 with the inclusion of 1% SFN. Furthermore, at any particular time during the crystallization, the number of spherulites for D1.4/SFN(1.0) is always larger than that of the D1.4 neat specimen (Fig. 5b). The total number of spherulites increased ~ 4.7 times (from 9 to 42). In addition, the

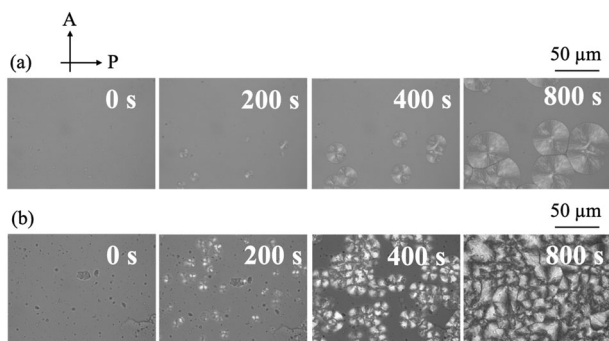
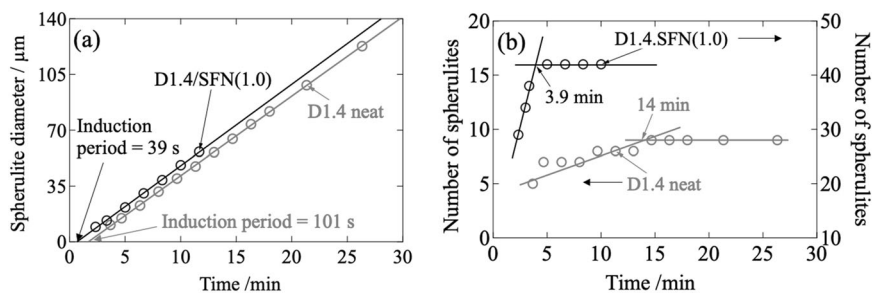


Fig. 4 POM images as a function of time for crystallization at 120 °C for **a** D1.4 neat **b** D1.4/SFN(1.0) specimens

Fig. 5 a Spherulite diameter and **b** the number of spherulites formed during isothermal crystallization at 120 °C evaluated from the POM images shown in Fig. 4



induction period was shortened from 101 to 39 s (Fig. 5a). However, the growth rate of the spherulites was unchanged (5 $\mu\text{m}/\text{min}$) by the addition of SFN (Fig. 5a). These results clearly show that SFN can enhance nucleation. SFN is considered to provide sites for easy formation of PLLA nuclei.

Determination of the equilibrium melting temperature (T_m^0)

The equilibrium melting temperature (T_m^0) is defined as a melting temperature (T_m) of infinitely thick lamella. T_m^0 is one of the most important thermodynamic parameters for determining the driving force (quench depth, $\Delta T = T_m^0 - T_c$) for the crystallization of polymers. T_m^0 values of the D1.4 neat, D1.4/SFN(1.0), D0.5 neat, and D0.5/SFN(1.0) specimens were evaluated by the Hoffman–Weeks plot [20]. As mentioned in the experimental section, the melting temperature was measured in the heating scan (heating rate = 10 °C/min) after crystallizing the specimens at the different isothermal temperatures. As shown in Fig. 6, the obtained melting temperature was plotted as a function of the crystallization temperature. The T_m^0 values for the D1.4 neat and D0.5 neat specimens were 180.7 °C and 193.3 °C, respectively. The lower value of T_m^0 for the D1.4 neat specimen is due to the presence of the D moiety, which causes the impurity effect for PLLA crystallization,

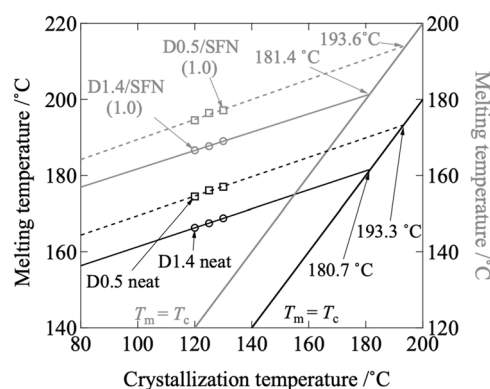


Fig. 6 Hoffman–Weeks plots for the determination of the equilibrium melting temperature

Fig. 7 **a** Heat flow as a function of time during isothermal crystallization at 110 °C and **b** degree of crystallinity (ϕ_{DSC}) as a function of time, which was evaluated based on the heat flow results

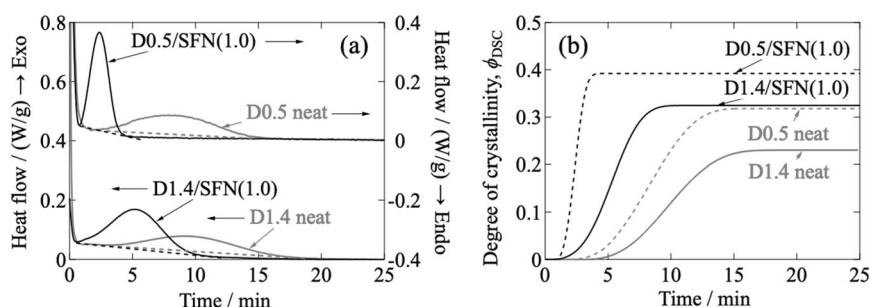
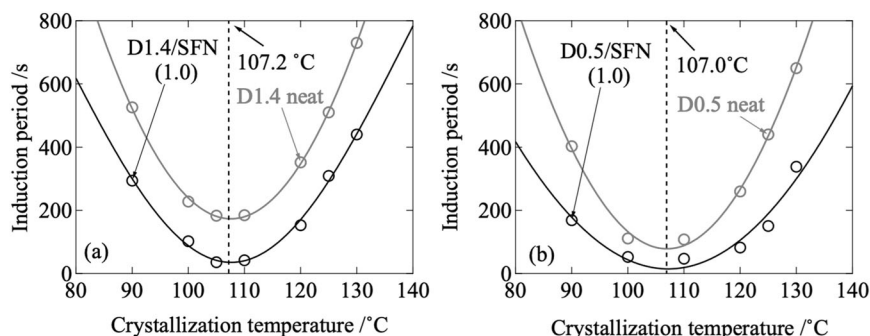


Fig. 8 Plots of the induction period as a function of crystallization temperature for **a** D1.4 specimens and **b** D0.5 specimens



resulting in the melting point depression. For the effect of SFN, there is a trivial difference in T_m^0 .

Isothermal crystallization by DSC

Figure 7 shows the DSC results of the isothermal crystallization of neat and 1% SFN included specimens at 110 °C. In Fig. 7a, the heat flow as a function of time at the T_{iso} of 110 °C is plotted. Adding 1% SFN, the crystallization isotherm curves were shifted to shorter times, showing an enhancement in the crystallization speed. Figure 7b shows the plots of the degree of crystallinity (ϕ_{DSC}) as evaluated based on the heat flow results using the following equation

$$\phi_{DSC}(t) = \frac{\int_0^t H(t)dt}{\Delta H_m^0}, \quad (1)$$

where t denotes time, and ΔH_m^0 is the enthalpy of fusion for the 100% crystal of PLLA. The value of ΔH_m^0 is taken as 93 J/g, following reference [21].

Figure 7b clearly indicates that the induction period was reduced and the final degree of crystallinity was increased by the presence of SFN. Maximum achievable crystallinity was found in the case of D0.5/SFN(1.0). In Fig. 8, the induction period is plotted as a function of the crystallization temperature. The graph shows a parabolic curve thereby producing a minimum induction period, $t_{0,min}$.

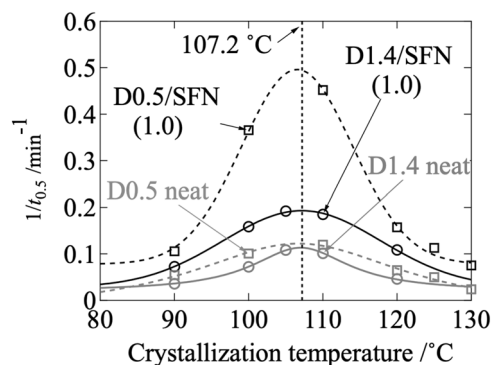
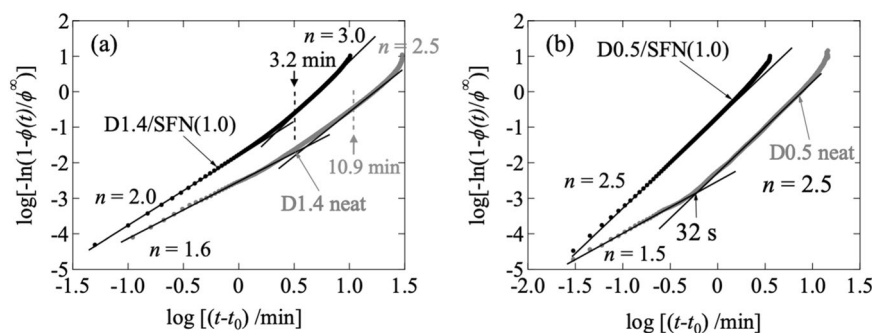


Fig. 9 Inverse of the crystallization half-time ($t_{0.5}$) as a function of the crystallization temperature, calculated from the DSC results (Fig. 7b)

was found at a temperature of 107.2 °C for the D1.4 specimens and 107.0 °C for the D0.5 specimens. The induction period was significantly reduced with the inclusion of SFN at all the crystallization temperatures investigated in this study. However, the temperature at $t_{0,min}$ was not affected by the inclusion of SFN.

Judging from the slope of the plot in Fig. 7b at $t_{0.5}$ (the crystallization half-time where the crystallinity reaches half of the final crystallinity), it was found that the crystallization of PLLA was accelerated by the addition of 1% SFN. The inverse $t_{0.5}$ can be used for the discussion of the crystallization rate, which is plotted as a function of the crystallization temperature in Fig. 9. As shown in Fig. 9, the overall crystallization growth rate was significantly

Fig. 10 Avrami plots at 110 °C based on DSC results for **a** D1.4 specimens and **b** D0.5 specimens



increased by the inclusion of SFN. Similar to the results of Fig. 8, a maximum crystallization rate, $1/t_{0.5,\text{max}}$, was observed at 107.2 °C for all of the specimens.

It should be noted that for both specimens D1.4 and D0.5, the crystallization rate and the induction period showed the same tendency, as the most effective temperature is ~107 °C, although the T_m^0 differs. Similar results have been reported in a review paper [1], where they explained the effect of the D moiety on the crystallization rate of PLLA. They reported that the crystallization of PLLA from the melt reaches a maximum in the temperature range of 105–110 °C, irrespective of the D moiety. This fact clearly indicates that the crystallization of PLLA is mainly governed by the kinetic driving force ($T - T_g$) rather than the thermodynamic driving force ($T_m^0 - T$). It should be noted here that the spherulite growth rate does not change in the presence of SFN (Fig. 5a), while $1/t_{0.5}$ is increased. The reason for the enhancement of $1/t_{0.5}$ can be attributed to the increased number of nuclei due to the addition of SFN (Fig. 5b). The enhanced nucleation of PLLA by SFN may be ascribed to the plausible formation of hydrogen bonding between the C=O group in PLLA and the N–H group of poly(L-alanine) (see the chemical structure in Fig. 1).

The kinetics of isothermal crystallization are described by the well-known Avrami theory [22–24], according to which the degree of crystallinity as a function of time $[\phi(t)]$ can be expressed as:

$$\frac{\phi(t)}{\phi^\infty} = 1 - \exp[-k(t - t_0)^n] \quad (2)$$

$$\log \left[-\ln \left(1 - \frac{\phi(t)}{\phi^\infty} \right) \right] = n \log(k) + n \log(t - t_0). \quad (3)$$

Here, ϕ^∞ denotes the degree of crystallinity after the complete crystallization, t_0 is the induction period for the crystallization, n is the Avrami exponent, which represents the dimensionality of growing crystallites, and k is the crystallization rate constant, which contains contributions from the nucleation and growth of crystal. The Avrami plots for the D1.4 neat, D1.4/SFN(1.0), D0.5 neat, and D0.5/SFN

(1.0) specimens are shown in Fig. 10. As shown in Fig. 10 a, b, the initial slopes of the Avrami plots were different from those of the later stages, suggesting a change in the mode of crystallization. The crossover time is earlier for the D0.5 neat specimen than the D1.4 neat specimen. However, in the case of the D0.5/SFN(1.0) specimen, such crossover behavior was not observed.

In the early stage of the crystallization, the Avrami exponents (n) for the D1.4 neat specimen and for the D0.5 neat specimen were both $n = 1.5$ – 1.6 . As shown in Fig. 5b, in the early stage of crystallization for the D1.4 neat and D1.4/SFN(1.0) specimens, the number of spherulites increased more or less linearly with time. Note here that the vertical broken lines shown in Fig. 10a indicate crossover times from homogeneous to heterogeneous nucleation based on the results shown in Fig. 5b after the subtraction of t_0 . Therefore, homogeneous nucleation can be considered. Then, $n = 1.6$ or $n = 2.0$ suggests a somewhat one-dimensional crystal growth. In the later stages of crystallization, the Avrami exponent n was increased to $n = 2.5$ for the D1.4 neat specimen, or $n = 3.0$ for the D1.4/SFN(1.0) specimen. The former result ($n = 2.5$ for the D1.4 specimen) may suggest between one-dimensional and two-dimensional crystal growth because of homogeneous nucleation (see Fig. 5b for $t < 14$ min). In contrast, the latter result ($n = 3.0$ for the D1.4/SFN(1.0) specimen) indicates almost three-dimensional crystal growth because of heterogeneous nucleation (see Fig. 5b for $t > 3.9$ min) due to the effect of adding SFN. Such a crossover was also confirmed for the D0.5 neat specimen, although the value of n is slightly smaller ($n = 2.5$). For the D0.5/SFN(1.0) specimen, no such crossover may suggest that the crystal growth is between two-dimensional and three-dimensional from the beginning of the crystallization where heterogeneous nucleation is dominant due to the effect of adding SFN.

Conclusions

The crystallization behavior of neat PLLA and PLLA/SFN (1%) specimens was investigated using POM and DSC. The

bionanocomposites of PLLA and SFN were prepared by solution casting. The results showed that SFN loading caused the acceleration of nucleation and an increase in the ultimate degree of crystallinity. Furthermore, the induction period was shortened and the spherulite density was increased. In contrast, there was no influence on the growth rate of the spherulites. The equilibrium melting temperature was unchanged. The dimensionality of the crystal growth was increased due to the inclusion of SFN. The temperature at which the crystallizability was the best did not change for any of the specimens examined in this study (D0.5 and D1.4, irrespective of SFN loading). From these results, we concluded that the driving force for the crystallization of PLLA is ascribed to kinetics ($T - T_g$) rather than thermodynamics ($T_m^0 - T$).

Acknowledgements This study was partially supported by a Grant-in-Aid for Challenging Exploratory Research with grant number 18K19115 from the Ministry of Education, Culture, Sports, Science, and Technology of Japan.

Compliance with ethical standards

Conflict of interest The authors declare that there is no conflict of interest.

Publisher's note: Springer Nature remains neutral with regard to jurisdictional claims in published maps and institutional affiliations.

References

- Saeidlou S, Huneault MA, Li H, Park CB. Poly(lactic acid) crystallization. *Prog Polym Sci*. 2012;37:1657–77.
- Kolstad JJ. Crystallization kinetics of poly(L-lactide-co-mesolactide). *J Appl Polym Sci*. 1996;62:1079–91.
- Xu JZ, Zhang ZJ, Xu H, Chen JBin, Ran R, Li ZM. Highly enhanced crystallization kinetics of poly(L-lactic acid) by poly(ethylene glycol) grafted graphene oxide simultaneously as heterogeneous nucleation agent and chain mobility promoter. *Macromolecules*. 2015;48:4891–4900.
- Picard E, Espuche E, Fulchiron R. Effect of an organo-modified montmorillonite on PLA crystallization and gas barrier properties. *Appl Clay Sci*. 2011;53:58–65.
- Barrau S, Vanmansart C, Moreau M, Addad A, Stoclet G, Lefebvre JM, et al. Crystallization behavior of carbon nanotube-poly(lactide) nanocomposites. *Macromolecules*. 2011;44:6496–502.
- Xu JZ, Chen T, Yang CL, Li ZM, Mao YM, Zeng BQ, et al. Isothermal crystallization of poly(L-lactide) induced by graphene nanosheets and carbon nanotubes: a comparative study. *Macromolecules*. 2010;43:5000–8.
- Pei A, Zhou Q, Berglund LA. Functionalized cellulose nanocrystals as biobased nucleation agents in poly(L-lactide) (PLLA)—Crystallization and mechanical property effects. *Compos Sci Technol*. 2010;70:815–21.
- Li H, Huneault MA. Effect of nucleation and plasticization on the crystallization of poly(lactic acid). *Polymer*. 2007;48:6855–66.
- Thi Ngoc Diep P, Mochizuki M, Doi M, Takagi H, Shimizu N, Igarashi N, et al. Effects of a special diluent as an agent of improving the crystallizability of poly(L-lactic acid). *Polym J*. 2019;51:283–94.
- Lucas F, Shaw JTB, Smith SG. Comparative studies of fibroins I. The amino acid composition of various fibroins and its significance in relation to their crystal structure and taxonomy. *J Mol Biol*. 1960;2:339–49.
- Patwa R, Soundararajan N, Mulchandani N, Bhasney SM, Shah M, Kumar S, et al. Silk nano-discs: a natural material for cancer therapy. *Biopolymers*. 2018;109:23231.
- Patwa R, Kumar A, Katiyar V. Effect of silk nano-disc dispersion on mechanical, thermal, and barrier properties of poly(lactic acid) based bionanocomposites. *J Appl Polym Sci*. 2018;135:46671.
- Patwa R, Kumar A, Katiyar V. Crystallization kinetics, morphology, and hydrolytic degradation of novel bio-based poly(lactic acid)/crystalline silk nano-discs nanobiocomposites. *J Appl Polym Sci*. 2018;135:46590.
- Tsuji H, Ishizaka T. Blends of aliphatic polyesters. VI. Lipase-catalyzed hydrolysis and visualized phase structure of biodegradable blends from poly(ϵ -caprolactone) and poly(L-lactide). *Int J Biol Macromol*. 2001;29:83–89.
- Kawai T, Rahman N, Matsuba G, Nishida K, Kanaya T, Nakano M, et al. Crystallization and melting behavior of poly(L-lactic acid). *Macromolecules*. 2007;40:9463–9.
- Pan P, Kai W, Zhu B, Dong T, Inoue Y. Polymorphous crystallization and multiple melting behavior of poly(L-lactide): Molecular weight dependence. *Macromolecules*. 2007;40:6898–905.
- Pan P, Zhu B, Kai W, Dong T, Inoue Y. Polymorphic transition in disordered poly(L-lactide) crystals induced by annealing at elevated temperatures. *Macromolecules*. 2008;41:4296–304.
- Zhang J, Tashiro K, Domb AJ, Tsuji H. Confirmation of disorder α form of poly(L-lactic acid) by the X-ray fiber pattern and polarized IR/Raman spectra measured for uniaxially-oriented samples. *Macromol Symp*. 2006;242:274–8.
- Zhang J, Tashiro K, Tsuji H, Domb AJ. Disorder-to-order phase transition and multiple melting behavior of poly(L-lactide) investigated by simultaneous measurements of WAXD and DSC. *Macromolecules*. 2008;41:1352–7.
- Hoffman JD, Weeks JJ. Melting process and the equilibrium melting temperature of polychlorotrifluoroethylene. *J Res Natl Bur Stand Sect A Phys Chem*. 1962;66A:13–28.
- Tsuji H, Ikada Y. Properties and morphologies of poly(L-lactide): 1. Annealing condition effects on properties and morphologies of poly(L-lactide). *Polymer*. 1995;36:2709–16.
- Avrami M. Kinetics of phase change. I General theory. *J Chem Phys*. 1939;7(12):1103–12.
- Avrami M. Kinetics of phase change. II transformation—time relations for random distribution of nuclei. *J Chem Phys*. 1940;8(2):212–24.
- Avrami M. Kinetics of phase change. III: granulation, phase change and microstructure. *J Chem Phys*. 1941;9:177–84.